applied sciences

MDPI

Article

Femtosecond Pulse Laser Near-Field Ablation of Ag Nanorods

Dezhi Zhu and Jianfeng Yan *

Department of Mechanical Engineering, Tsinghua University, Beijing 100084, China; zdz18@mails.tsinghua.edu.cn

* Correspondence: yanjianfeng@tsinghua.edu.cn

Received: 4 January 2019; Accepted: 18 January 2019; Published: 22 January 2019

Abstract: Ag nanorods (Ag NRs) with a mean aspect ratio of 3.9 were prepared through a wet-chemical method, and the absorption spectra for various aspect ratios were obtained. The morphology transformation of Ag NRs irradiated with a femtosecond pulse laser was investigated through transmission electron microscopy (TEM). The near-field ablation was dependent on the laser polarization and wavelength. Laser-induced high electric field intensity was observed at the ends, middle, and junctions of the Ag NRs under various ablation conditions. Through simulation, the evolution mechanism was analyzed in detail. The effect of laser polarization angle on plasmonic junction welding was also investigated. By controlling the electronic field distribution, several nanostructures were obtained: bone-shaped NRs, T-shaped NRs, dimers, trimers, curved NRs, and nanodots. This study suggests a potentially useful approach for the reshaping, cutting, and welding of nanostructures.

Keywords: Ag nanorods; femtosecond pulse laser; near-field ablation; polarization

1. Introduction

Because of their wide range of potential applications in biomedicine [1,2], analytical chemistry [3,4], and photovoltaics [5], plasmonic nanoparticle research is an attractive field [6–8]. Silver nanoparticles (Ag NPs) play an essential role in catalysts because of their high thermal conductivity [9]. Surface plasmon resonance (SPR) is a crucial property and originates from the collective oscillation of surface free electrons under the coupling of light and plasmonic NPs [10]. The SPR band of Ag NPs is dependent on their optical properties, which are sensitive to NP morphology and size [11]. Ultrafast laser ablation is crucial for controlling morphology and has therefore been extensively investigated [12].

Exposure of Ag NPs to single- and multiple-pulse lasers results in ablation [13–15], and three mechanisms were proposed for interpreting this ablation process [16]. Takami et al. attributed the fragmentation of NPs to laser-induced thermal evaporation and confirmed that fragmentation occurs only if the NPs have a temperature higher than their boiling point [17]. Yamaguchi et al. conducted a pulsed laser ablation experiment using a laser at wavelength of 355 nm, and concluded that NPs were fragmented layer by layer under the photothermal effect [18]. In support of the thermal evaporation mechanism, Alexander et al. performed an experiment and combined the results with melting calculations, concluding that the mechanism is valid when using a laser of low intensity [19]. In contrast, Hartland et al. adopted the Coulomb explosion mechanism, which considers fragmentation to result from charge repulsion caused by the ejection of numerous free electrons; in pulsed laser ablation of Ag NPs, hydrated electrons were detected [20]. Subsequently, Muto et al. conducted 355 nm nanosecond laser ablation of NPs and also observed hydrated electrons and charged ions. The results indicated that although the wavelength of 355 nm is not in the SPR band, fast absorption of interband electrons enhanced fragmentation [21]. Furthermore, Marsili et al. performed picosecond laser-induced fragmentation of NPs using two temperature modes and concluded that Coulomb explosion plays a larger role than does laser-induced thermal evaporation [22].

In addition to the two aforementioned mechanisms, a near-field ablation mechanism based on plasmonic field enhancement has been proposed; this process would be nonthermal excitation because the ablation temperature is lower than the melting point [23,24]. Perez et al. reported that the photomechanical effect can result in ablation without a thermal phase transformation, and the thermoelastic stress can overcome the physical strength of NPs [25]. Sakai et al. conducted laser ablation of a single NP on a silicon substrate, and two lobe-shaped structures were observed that matched the enhanced field distribution [26]. Kolloch et al. discussed the complicacy of the near-field distribution on the basis of ultrafast laser ablation of gold nanotriangles [27].

The modification of various substrates through laser-induced near-field ablation has been widely investigated [28,29]. However, in most research, the NPs have completely destroyed and removed from the substrates after a single high-intensity pulse. Little information presently exists on the morphology evolution of silver nanorods (Ag NRs) subject to near-field ablation. In this study, we demonstrated the dependence of the near-field distribution on laser wavelength and polarization by performing a femtosecond pulse laser ablation experiment, achieving Ag NRs morphology control by tuning the electronic field distribution. The evolution mechanism was analyzed through both experimentation and simulation. In addition, the effect of the laser polarization angle on junction plasmonic welding was also determined. Furthermore, this study proposes a useful tool for fabricating nanostructures, including bone-shaped NRs, T-shaped NRs, and nanodots.

2. Experimental

Ag NRs were synthesized through a wet-chemical method [30]. First, 25 mL of 0.4 mM $AgNO_3$ (>99.8%, Sinopharm Chemical Reagent Co., Ltd) solution was added to 25 mL of 2 mM sodium dodecyl sulfonate (>99%, Sinopharm Chemical Reagent Co., Ltd) solution. Subsequently, 4 mL of 10 mM trisodium citrate (>99%, Beijing Harveybio Gene Technology Co., Ltd) solution was added. The mixture was stirred for 80 min at 90 °C, and the solution became turbid and gray–green.

Figure 1 shows a schematic of the experimental setup for irradiation of Ag NRs using a femtosecond pulse laser. A 35 fs laser pulse was emitted by an amplified Ti–sapphire laser system, and the repetition rate was 1 kHz, with a central wavelength of 800 nm. Ag NRs, dropped onto carbon film, were irradiated at non-focused femtosecond-pulsed spots with a diameter of 5 mm. The exposure time was controlled using a shutter connected to a computer, and the laser fluence was fixed by an attenuator at 2 mJ/cm^2. The laser polarization and wavelength were adjusted using a half-wave plate and frequency doubling crystal (BBO crystal). Transmission electron microscopy (TEM) images were acquired using an FEI Tecnai G2 F20 operated at 120 kV. The Ag NRs were centrifuged three times and dropped onto copper grids (400 mesh) coated with ultrathin carbon film.

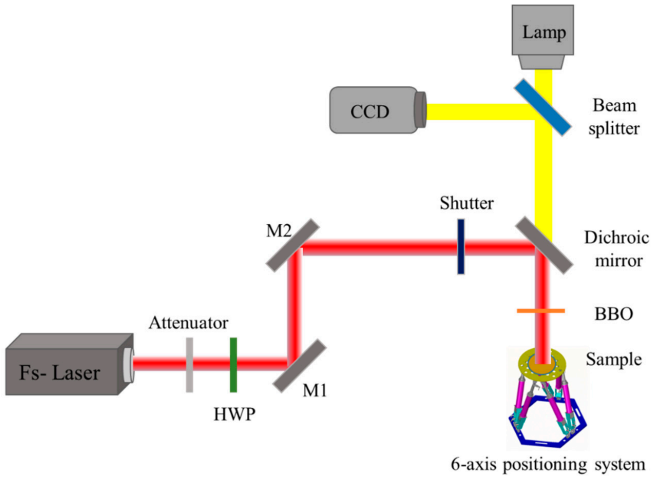

Figure 1. Schematic of experimental setup for irradiation of Ag NRs using a femtosecond pulse laser. Mirrors (M1, M2). Half-wave plate (HWP).

3. Results and Discussion

After femtosecond pulse laser irradiation, various Ag nanostructures were obtained. Figure 2a shows a TEM image of Ag NRs after plasmon-induced melting at parallel polarization. The end of the Ag NR had melted into a spherical structure with a diameter of 50 nm. This indicates that a temperature gradient was caused by the near-field ablation [31]. Figure 2b shows the transition from as-prepared NRs to small NRs with perpendicular polarization, and numerous nanodots were observed in the vicinity of the NR. This suggests that the NRs were split into small clusters because the electric field was sufficiently high. Figure 2c reveals the transition from a nanosphere into a bone-shaped NR, and this morphology is in agreement with an enhanced plasmonic field distribution that results from the SPR associated with laser polarization [32]. Greater electric field enhancement was expected for smaller nanospheres because larger nanospheres have larger scattering contributions. In addition, the multipole oscillations of the large nanospheres resulted in a distorted dipole field distribution. As illustrated in Figure 2d, a nanojoint between two adjacent Ag NRs formed through melting and fusion without any additional filler because of the strong electronic field generated in the gap between them. T-shaped NRs play a crucial role in optical logic gates [33] and temperature-sensitive devices [34], and they were optimized through adjustment of the laser polarization angle in this study.

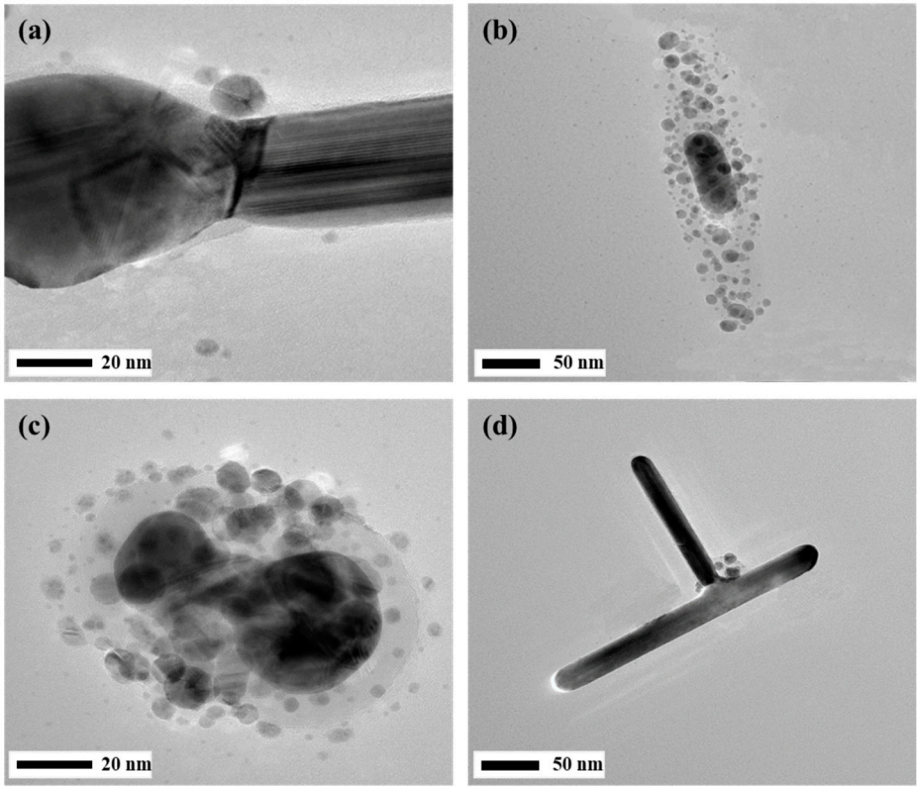

Figure 2. Morphology of Ag NPs after femtosecond pulse laser illumination. (**a**) Melting occurred at the ends of the Ag NRs, and a grain boundary was evident. (**b**) TEM image of the transformation from as-prepared NRs into small NRs. (**c**) TEM image of the transformation from nanospheres into bone-shaped NRs. (**d**) Melting occurred at the junction between two adjacent rods. The scale bars are 20 and 50 nm.

3.1. Controlling the Morphology of Ag NRs by Tuning the Laser Polarization and Wavelength

Figure 3a shows a TEM image of an as-prepared Ag NR before laser ablation. The mean aspect ratio of the Ag NRs was 3.9 and could be controlled by modifying the concentration of the trisodium citrate solution. The surface plasmons of the NRs were divided into two distinct modes—transverse and longitudinal—because of light polarization. To analyze the relationship between the extinction

peak wavelength and NR aspect ratio, Mie–Gans theory was considered, and the extinction coefficient γ for Ag NRs was calculated using the dipole approximation as follows [35]:

$$\gamma = \frac{2\pi NV\varepsilon_{\mathrm{m}}^{3/2}}{3\lambda}\sum_{j}\frac{(1/p_j^2)\varepsilon_2(\omega)}{(\varepsilon_1(\omega)+(1-p_j)\varepsilon_m/p_j)^2+\varepsilon_2(\omega)^2}, \quad (1)$$

$$p_A = \frac{1-e^2}{e^2}\left(\frac{1}{2e}\ln\left(\frac{1+e}{1-e}\right)-1\right), \quad (2)$$

$$p_B = p_C = \frac{1-p_A}{2}, \quad (3)$$

$$e = \sqrt{1-\left(\frac{B}{A}\right)^2}, \quad (4)$$

where N and V are the number of nanoparticles per unit volume and the volume of single particle, respectively; ε_m, ε_1, and ε_2 represent the dielectric constant of medium, the real, and complex part of the material dielectric function, respectively; p_j are the depolarization factors of the nanorod axes (A, B, C). The aspect ratio R is A/B, and λ is the laser wavelength.

The relationship between the extinction coefficient and light wavelength at three aspect ratios is plotted in Figure 3b. The extinction peak wavelength of the longitudinal mode increased with increasing Ag NR aspect ratio, and the resonance band was much more pronounced at the highest ratio, with 120 nm width. This calculated result was in agreement with an analysis of plasmonic NPs [36]. Conversely, the extinction peak wavelength of the transverse mode was blueshifted with increased aspect ratio, and the extinction coefficient was almost constant. In addition, the rising shoulder at lower wavelengths (less than 360 nm) corresponds to interband absorption between the 4d and 5sp bands [37]. When the aspect ratio was 3.9, the transverse plasmon absorption peak wavelength was 380 nm, and the longitudinal plasmon resonance peak was 790 nm.

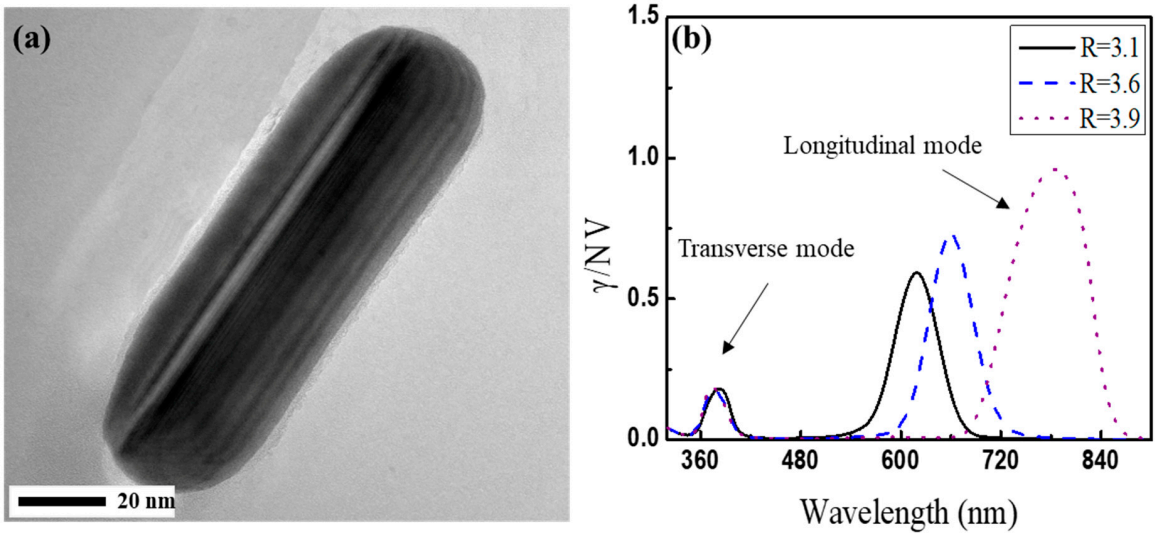

Figure 3. (**a**) TEM image of as-prepared Ag NR; the mean aspect ratio of all NRs was 3.9. The scale bar is 20 nm. (**b**) Calculated extinction spectra of Ag NRs with varying aspect ratios R. For R = 3.9, the transverse plasmon absorption band was at 380 nm, whereas the longitudinal plasmon resonance band was at 790 nm.

When using parallel polarization and 800 nm wavelength, which is near the longitudinal plasmon resonance band, a dipolar lobe morphology of the Ag NRs after illumination was observed, as shown in Figure 4a. This indicated that ablation occurred only at the ends, but not on the two sides, of the

NRs, because small clusters formed at the ends under the enhanced electronic field. This agrees with the simulation results presented in Figure 4b, and the enhancement factor was 13. As illustrated in Figure 4c, a notch in the middle of the NRs could be observed when using parallel polarization and 400 nm laser wavelength, which is far from the longitudinal plasmon resonance band. Thus, greater ablation occurred in the middle of the NRs than at any other part, and the electronic field had the distribution displayed in Figure 4d. Off-resonant excitation resulted from multipolar oscillation, which was related to the wavelength of the laser and size of the nanostructures [38]. By adjusting the laser wavelength, the enhanced electronic field distribution could be shifted along the NR. Thus, the ablation morphology of the NRs was controllable. Although the enhancement factor was small, the enhanced field could yield intense ablation under the effect of multiple femtosecond laser pulses. With perpendicular polarization and 800 nm laser wavelength, which is off-transverse resonant excitation, small clusters formed on the two sides of the Ag NRs, as indicated in Figure 4e. By analyzing the calculation results in Figure 4f, the electronic field at the two sides was found to be stronger than that at the ends of the NRs. Thus, the as-prepared NRs became elongated NRs under these processing conditions. Especially at the near-transverse resonance band of 400 nm in Figure 4g,h, smaller and thinner Ag NRs were obtained because of the higher enhancement factor of 4.3 than that at 800 nm wavelength. This suggests that some useful nanostructures can be obtained by adjusting the electronic field distribution.

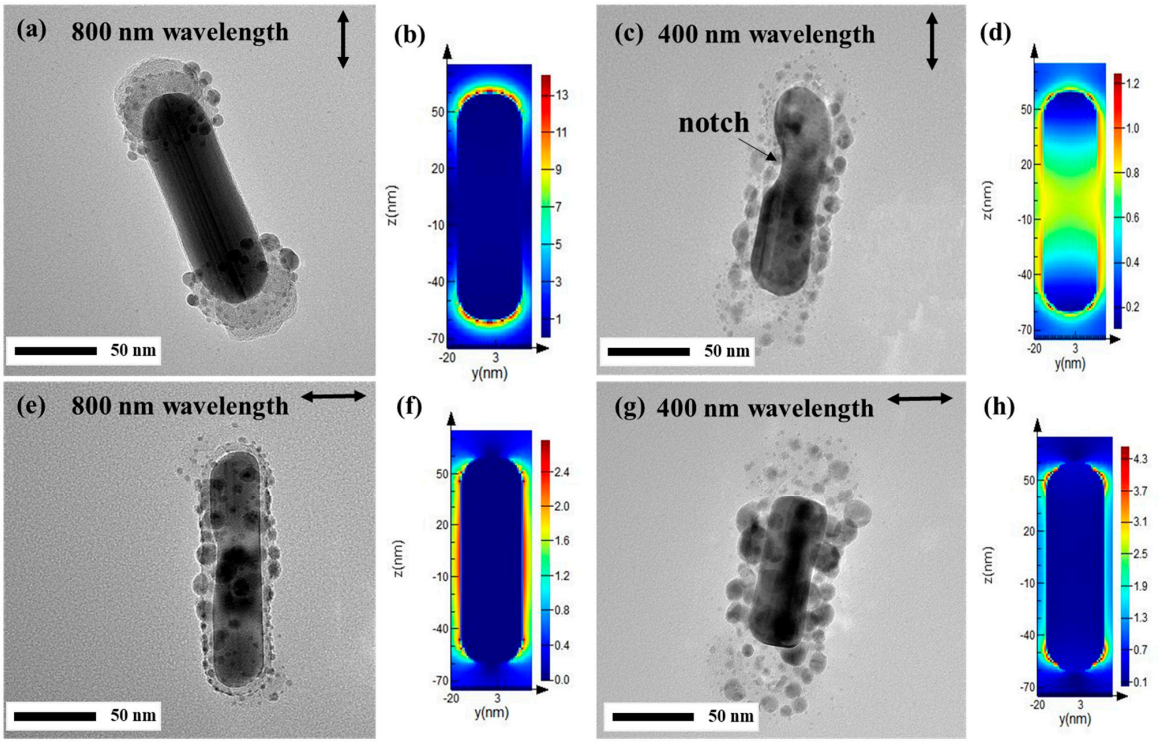

Figure 4. TEM images and corresponding calculated electric field distributions of Ag NRs after irradiation with lasers of different polarizations and wavelengths. (**a**,**b**) Ablation was observed at the ends of a Ag NR when parallel polarization and 800 nm laser wavelength were employed. (**c**,**d**) Ablation occurred at both the ends and sides of a Ag NR when parallel polarization and 400 nm laser wavelength were used. (**e**,**f**) Ablation was observed on the two sides when perpendicular polarization and 800 nm laser wavelength were employed. (**g**,**h**) Ablation occurred at the two sides when perpendicular polarization and 400 nm laser wavelength were used, and the electric field intensity was higher than that when 800 nm wavelength was used. The arrows indicate the laser polarization direction. The scale bar is 50 nm.

3.2. Near-Field Ablation Evolution of Ag NRs

Regarding the femtosecond pulse laser near-field ablation process, a possible thermo-force coupling mechanism was proposed based on the melting and curving of the Ag NRs. First, laser energy is absorbed by the electrons, and accumulated heat is then transferred from electrons to the lattice through electron–phonon coupling within 1–4 ps [39]. Strong excitation with large intensity can increase the time required for energy transfer to the lattice [28]. When the lattice temperature is higher than the boiling temperature of Ag NRs, fragmentation starts to occur. The near-field force caused by localized electronic field enhancement promotes fragmentation. As shown in Figure 5a,b, multipolar oscillation resulted in the formation of a notch, and the simulated electronic field in the middle of the Ag NR was enhanced when the next pulse arrived. Subsequently, the notched NR broke, yielding two small NRs, as illustrated in Figure 5c. Figure 5d shows the electronic field distribution of these two small NRs under the laser pulse effect, revealing that the field in the gap and at the middle was enhanced. This resulted in further fragmentation and nanodot formation, as indicated in Figure 5e. In addition, the fusion of small clusters was observed. Thus, small clusters fragmented from NRs were melted after laser illumination and subsequently agglomerated. The effect of the electric field caused by the small clusters on the ablation process was not taken into account in this study, because it was not the main factor behind the fragmentation of NRs. As indicated in Figure 5f,g, under the near-field force effect, the NR with a notch was curved because of the electronic field gradient, and the force was sufficiently strong to remove the NPs [40]. Figure 5h,i show the further fragmentation of the dimer and subsequent formation of nanodots.

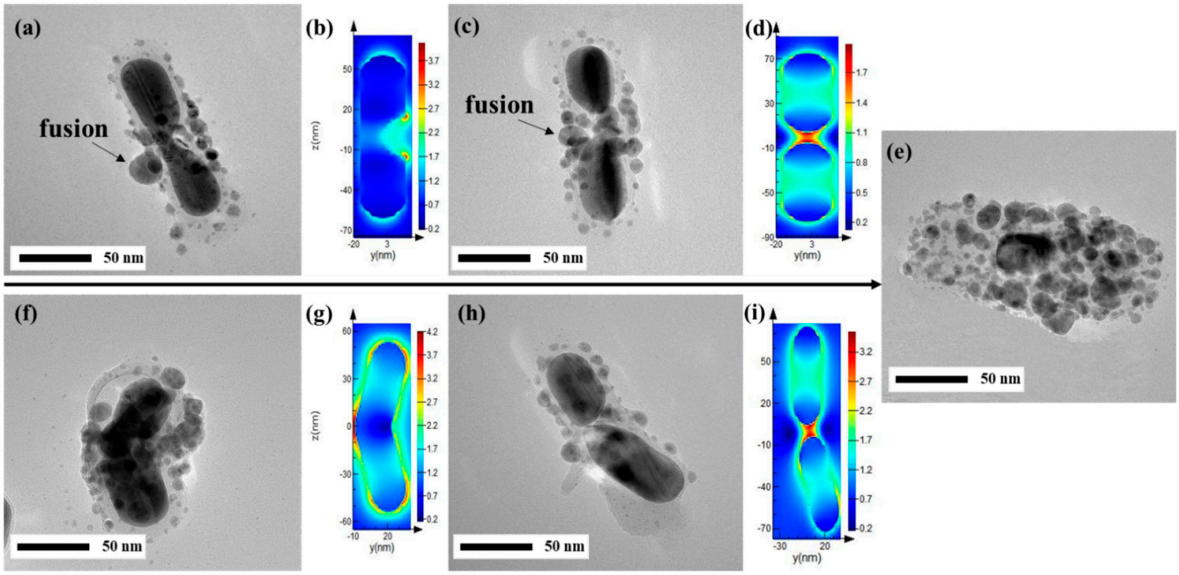

Figure 5. Schematic of the morphology evolution from NRs to nanodots. Corresponding TEM images and calculated electric field distributions of Ag NRs after irradiation with light of wavelength 400 nm. (**a**,**b**) The middle section of the material was ablated, and the electric field was enhanced in this area. (**c**,**d**) This resulted in separation into two small NRs and ablation enhancement in each particle. (**e**) Finally, nanodots were obtained. Another possible evolution process is also proposed. (**f**,**g**) Electric field gradient induced bending of Ag NRs, with the intensity enhanced in the middle. (**h**,**i**) This resulted in fragmentation and separation. The scale bar is 50 nm.

Nanojoints between two metal structures have been widely studied, such as end to end junction and side to side junction [41,42]. However, side-to-end T-shaped junctions have rarely been reported. The success of plasmonic welding is dependent on the gap and angle between the two metal structures, and perpendicular structures have superior bonding [43]. Through femtosecond laser near-field ablation of two noncontact Ag NRs, T-shaped nanojoints were obtained. As displayed in Figure 6a,

the angle between the two NRs was 90°, and the laser polarization angle was 45° along the NR. Figure 6c illustrates the calculated electronic field under these conditions, and the field was found to differ from the field of a single NR because of field coupling between the NRs. The field in the gap was enhanced and symmetric. Because of the intense field in the gap, the material near the gap melted and then flowed into the gap and fused. Some small clusters were observed around the nanojoint because of material explosion. Figure 6b,d presents the asymmetric field distribution in the gap, which may have resulted in inhomogeneous melting and could have weakened the bonding. As displayed in Figure 6e, the field on the other side of the NR was enhanced and could destroy the structure of the NR. This indicates that plasmonic welding of T-shaped NRs is dependent on the polarization direction related to the spatial structure of the NRs.

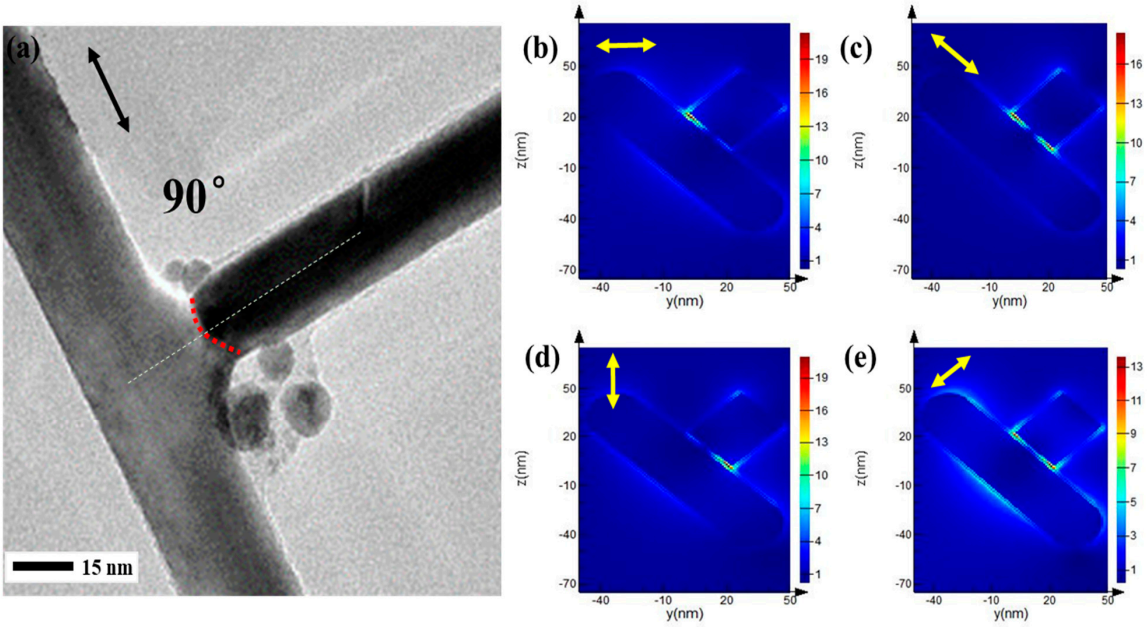

Figure 6. (**a**) TEM image of plasmonic welding at a Ag NR junction. The scale bar is 15 nm. The red dashed line is the nanojoint contour. Corresponding calculated electric field distributions of Ag NRs irradiated with 400 nm laser light and polarization angles (**b**) 0°, (**c**) 45°, (**d**) 90°, and (**e**) 135°. The angle between the two NRs was 90°, and the gap was 4 nm. The arrows indicate the laser polarization direction. The color scales represent the electronic field intensity.

4. Conclusions

In this study, we conducted femtosecond laser near-field ablation of Ag NRs with an average aspect ratio of 3.9. Dependence of the ablation morphology on the laser polarization direction and wavelength was observed. When the laser polarization was parallel to the long axis of the NR and a laser of 800 nm wavelength was used, the electronic field was enhanced at the ends of the NR, where fragmentation occurred, leading to a lobe-shaped morphology. When 400 nm wavelength excitation was employed, multipolar oscillation induced field enhancement in the middle of the NR, yielding a notch. By contrast, when the laser polarization was perpendicular to the long axis of the NR, material along the two sides was ablated, and small clusters formed because of the transverse excitation. By adjusting the electronic field distribution, useful nanostructures can be obtained. In addition, the near-field ablation evolution of Ag NRs was investigated, and a possible thermo-force coupling mechanism was proposed. During the transition from NRs to nanodots, small clusters were formed through thermal evaporation, and these clusters then melted and fused. The near-field force plays a critical role in ablation, and the notched NR was curved under the strong field gradient. Furthermore, the dependence of plasmonic welding of T-shaped NRs on polarization direction related to the spatial structure was determined. Only when the laser polarization was parallel to one of the two structures

was a strong nanojoint obtained because of the symmetric field distribution under the field coupling between the nanostructures. This study may promote the application of femtosecond laser ablation for the reshaping, cutting, and welding of nanostructures.

Author Contributions: Investigation, J.Y. and D.Z.; supervision, J.Y.; writing—original draft, J.Y. and D.Z.

Funding: This research was supported by the National Key Research and Development Program of China (2017YFB1104900, 2018YFB1107200) and the National Natural Science Foundation of China (Grant No. 51775303).

Acknowledgments: The authors would like to thank Professor Lan Jiang at the Beijing Institute of Technology, China.

Conflicts of Interest: The authors declare no conflict of interest.

References

1. Sokolov, K.; Follen, M.; Aaron, J.; Pavlova, I.; Malpica, A.; Lotan, R.; Richardskortum, R. Real-Time Vital Optical Imaging of Precancer Using Anti-Epidermal Growth Factor Receptor Antibodies Conjugated to Gold Nanoparticles. *Cancer Res.* **2004**, *63*, 1999.
2. Murphy, C.J.; Gole, A.M.; Stone, J.W.; Sisco, P.N.; Alkilany, A.M.; Goldsmith, E.C.; Baxter, S.C. Gold nanoparticles in biology: Beyond toxicity to cellular imaging. *Acc. Chem. Res.* **2008**, *40*, 1721–1730. [CrossRef] [PubMed]
3. Kneipp, J.; Kneipp, H.; Kneipp, K. SERS—A single-molecule and nanoscale tool for bioanalytics. *Chem. Soc. Rev.* **2008**, *37*, 1052–1060. [CrossRef] [PubMed]
4. Brus, L. Noble metal nanocrystals: Plasmon electron transfer photochemistry and single-molecule Raman spectroscopy. *Acc. Chem. Res.* **2008**, *41*, 1742. [CrossRef] [PubMed]
5. Kamat, P.V. Quantum Dot Solar Cells. Semiconductor Nanocrystals as Light Harvesters. *J. Phys. Chem. C* **2008**, *112*, 18737–18753. [CrossRef]
6. Darroudi, M.; Ahmad, M.B.; Zamiri, R.; Abdullah, A.H.; Ibrahim, N.A.; Shameli, K.; Husin, M.S. Preparation and characterization of gelatin mediated silver nanoparticles by laser ablation. *J. Alloys Compd.* **2011**, *509*, 1301–1304. [CrossRef]
7. Yan, J.; Zou, G.; Wu, A.-P.; Ren, J.; Yan, J.; Hu, A.; Zhou, Y. Pressureless bonding process using Ag nanoparticle paste for flexible electronics packaging. *Scr. Mater.* **2012**, *66*, 582–585. [CrossRef]
8. Hu, A.; Guo, J.Y.; Alarifi, H.; Patane, G.; Zhou, Y.; Compagnini, G.; Xu, C.X. Low temperature sintering of Ag nanoparticles for flexible electronics packaging. *Appl. Phys. Lett.* **2010**, *97*, 153117. [CrossRef]
9. Nakamura, T.; Magara, H.; Herbani, Y.; Sato, S. Fabrication of silver nanoparticles by highly intense laser irradiation of aqueous solution. *Appl. Phys. A* **2011**, *104*, 1021–1024. [CrossRef]
10. Hartland, G.V. Optical studies of dynamics in noble metal nanostructures. *Chem. Rev.* **2011**, *111*, 3858–3887. [CrossRef]
11. Yeshchenko, O.A.; Dmitruk, I.M.; Alexeenko, A.A.; Losytskyy, M.Y.; Kotko, A.V.; Pinchuk, A.O. Size-dependent surface-plasmon-enhanced photoluminescence from silver nanoparticles embedded in silica. *Phys. Rev. B* **2009**, *79*, 1377–1381. [CrossRef]
12. Akman, E.; Oztoprak, B.G.; Gunes, M.; Kacar, E.; Demir, A. Effect of femtosecond Ti:Sapphire laser wavelengths on plasmonic behaviour and size evolution of silver nanoparticles. *Photonics Nanostruct. Fundam. Appl.* **2011**, *9*, 276–286. [CrossRef]
13. Giorgetti, E.; Marsili, P.; Muniz-Miranda, M.; Gellini, C.; Giammanco, F. Spectroscopic evidence of positive clusters in Ag colloids obtained by laser ablation in aqueous solutions. *Appl. Phys. A* **2014**, *117*, 327–331. [CrossRef]
14. Šmejkal, P.; Pfleger, J.; Vlčková, B. Study of laser fragmentation process of silver nanoparticles in aqueous media. *Appl. Phys. A* **2008**, *93*, 973–976. [CrossRef]
15. Werner, D.; Hashimoto, S. Improved Working Model for Interpreting the Excitation Wavelength- and Fluence-Dependent Response in Pulsed Laser-Induced Size Reduction of Aqueous Gold Nanoparticles. *J. Phys. Chem. C* **2016**, *115*, 5063–5072. [CrossRef]
16. Werner, D.; Furube, A.; Okamoto, T.; Hashimoto, S. Femtosecond Laser-Induced Size Reduction of Aqueous Gold Nanoparticles: In Situ and Pump-Probe Spectroscopy Investigations Revealing Coulomb Explosion. *J. Phys. Chem. C* **2011**, *115*, 8503–8512. [CrossRef]

17. Takami, A.; Kurita, H.; Koda, S. Laser-Induced Size Reduction of Noble Metal Particles. *J. Phys. Chem. B* **2003**, *103*, 1226–1232. [CrossRef]
18. Susumu, I.; Masakazu, S.; Yukio, Y. Bimodal Size Distribution of Gold Nanoparticles under Picosecond Laser Pulses. *J. Phys. Chem. B* **2005**, *109*, 9404.
19. Pyatenko, A.; Yamaguchi, M.; Suzuki, M. Mechanisms of Size Reduction of Colloidal Silver and Gold Nanoparticles Irradiated by Nd:YAG Laser. *J. Phys. Chem. C* **2009**, *113*, 9078–9085. [CrossRef]
20. Kamat, P.V.; Flumiani, M.; Hartland, G.V. Picosecond Dynamics of Silver Nanocluster. Photoejection of Electrons and Fragmentation. *J. Phys. Chem. B* **1998**, *102*, 2123–3128. [CrossRef]
21. Muto, H.; Miyajima, K.; Mafuné, F. Mechanism of Laser-Induced Size Reduction of Gold Nanoparticles As Studied by Single and Double Laser Pulse Excitation. *J. Phys. Chem. C* **2008**, *112*, 5810–5815. [CrossRef]
22. Giammanco, F.; Giorgetti, E.; Marsili, P.; Giusti, A. Experimental and Theoretical Analysis of Photofragmentation of Au Nanoparticles by Picosecond Laser Radiation. *J. Phys. Chem. C* **2010**, *114*, 3354–3363. [CrossRef]
23. Plech, A.; Kotaidis, V.; Lorenc, M.; Boneberg, J. Femtosecond laser near-field ablation from gold nanoparticles. *Nat. Phys.* **2005**, *2*, 44–47. [CrossRef]
24. Plech, A.; Ibrahimkutty, S.; Reich, S.; Newby, G. Thermal dynamics of pulsed-laser excited gold nanorods in suspension. *Nanoscale* **2017**, *9*, 17284–17292. [CrossRef] [PubMed]
25. Danny, P.; Laurent, J.L. Ablation of solids under femtosecond laser pulses. *Phys. Rev. Lett.* **2002**, *89*, 255504.
26. Nedyalkov, S.; Miyanishi, O. Near field properties in the vicinity of gold nanoparticles placed on various substrates for precise nanostructuring. *J. Phys. D Appl. Phys.* **2006**, *39*, 5037. [CrossRef]
27. Kolloch, A.; Geldhauser, T.; Ueno, K.; Misawa, H.; Boneberg, J.; Plech, A.; Leiderer, P. Femtosecond and picosecond near-field ablation of gold nanotriangles: Nanostructuring and nanomelting. *Appl. Phys. A* **2011**, *104*, 793–799. [CrossRef]
28. Plech, A.; Leiderer, P.; Boneberg, J. Femtosecond laser near field ablation. *Laser Photonics Rev.* **2009**, *3*, 435–451. [CrossRef]
29. Harrison, R.K.; Adela, B.Y. Role of near-field enhancement in plasmonic laser nanoablation using gold nanorods on a silicon substrate. *Opt. Express* **2010**, *18*, 22556–22571. [CrossRef]
30. Hu, J.Q.; Chen, Q.; Xie, Z.X.; Han, G.B.; Wang, R.H.; Ren, B.; Zhang, Y.; Yang, Z.L.; Tian, Z.Q. A Simple and Effective Route for the Synthesis of Crystalline Silver Nanorods and Nanowires. *Adv. Funct. Mater.* **2010**, *14*, 183–189. [CrossRef]
31. Liu, L.; Peng, P.; Hu, A.; Zou, G.; Duley, W.W.; Zhou, Y.N. Highly localized heat generation by femtosecond laser induced plasmon excitation in Ag nanowires. *Appl. Phys. Lett.* **2013**, *102*, 073107. [CrossRef]
32. Hashimoto, S.; Werner, D.; Uwada, T. Studies on the interaction of pulsed lasers with plasmonic gold nanoparticles toward light manipulation, heat management, and nanofabrication. *J. Photochem. Photobiol. C Photochem. Rev.* **2012**, *13*, 28–54. [CrossRef]
33. Wei, H.; Wang, Z.; Tian, X.; Kall, M.; Xu, H. Cascaded logic gates in nanophotonic plasmon networks. *Nat. Commun.* **2011**, *2*, 387. [CrossRef] [PubMed]
34. Garnett, E.C.; Cai, W.; Cha, J.J.; Mahmood, F.; Connor, S.T.; Greyson Christoforo, M.; Cui, Y.; McGehee, M.D.; Brongersma, M.L. Self-limited plasmonic welding of silver nanowire junctions. *Nat. Mater.* **2012**, *11*, 241–249. [CrossRef] [PubMed]
35. Petryayeva, E.; Krull, U.J. Localized surface plasmon resonance: Nanostructures, bioassays and biosensing—A review. *Anal. Chim. Acta* **2011**, *706*, 8–24. [CrossRef] [PubMed]
36. Yan, B.; Yang, Y.; Wang, Y. Comment on "Simulation of the Optical Absorption Spectra of Gold Nanorods as a Function of Their Aspect Ratio and the Effect of the Medium Dielectric Constant". *J. Phys. Chem. B* **1999**, *107*, 315–319. [CrossRef]
37. Solati, E.; Mashayekh, M.; Dorranian, D. Effects of laser pulse wavelength and laser fluence on the characteristics of silver nanoparticle generated by laser ablation. *Appl. Phys. A* **2013**, *112*, 689–694. [CrossRef]
38. Ghenuche, P.; Cherukulappurath, S.; Taminiau, T.H.; van Hulst, N.F.; Quidant, R. Spectroscopic mode mapping of resonant plasmon nanoantennas. *Phys. Rev. Lett.* **2008**, *101*, 116805. [CrossRef]
39. Khlebtsov, N.G. Optics and biophotonics of nanoparticles with a plasmon resonance. *Quantum Electron.* **2008**, *38*, 504–529. [CrossRef]

40. Huang, W.; Qian, W.; El-Sayed, M.A. Gold nanoparticles propulsion from surface fueled by absorption of femtosecond laser pulse at their surface plasmon resonance. *J. Am. Chem. Soc.* **2006**, *128*, 13330–13331. [CrossRef]
41. Song, T.-B.; Chen, Y.; Chung, C.-H.; Yang, Y.; Bob, B.; Duan, H.-S.; Li, G.; Tu, K.-N.; Huang, Y.; Yang, Y. Nanoscale joule heating and electromigration enhanced ripening of silver nanowire contacts. *ACS Nano* **2014**, *8*, 2804–2811. [CrossRef] [PubMed]
42. Peng, P.; Hu, A.; Gerlich, A.P.; Zou, G.; Liu, L.; Zhou, Y.N. Joining of Silver Nanomaterials at Low Temperatures: Processes, Properties, and Applications. *ACS Appl. Mater. Interfaces* **2015**, *7*, 12597–12618. [CrossRef] [PubMed]
43. Lin, L.; Liu, L.; Peng, P.; Zou, G.; Duley, W.W.; Zhou, Y.N. In situ nanojoining of Y- and T-shaped silver nanowires structures using femtosecond laser radiation. *Nanotechnology* **2016**, *27*, 125201. [CrossRef] [PubMed]